Circadian protection against bacterial skin infection by epidermal CXCL14-mediated innate immunity

Kojiro Tsujihana[a,b,1] (ID), Kosuke Tanegashima[c,1] (ID), Yasuko Santo[a], Hiroyuki Yamada[a], Sota Akazawa[a] (ID), Ryuta Nakao[d], Keiko Tominaga[e], Risa Saito[c,f], Yasumasa Nishito[g], Ryu-Ichiro Hata[h] (ID), Tomonori Nakamura[i,j,k] (ID), Iori Murai[a], Yuka Kono[a], Maho Sugawa[a], Miki Tanioka[b], Gyohei Egawa[b] (ID), Masao Doi[a] (ID), Tadashi Isa[l] (ID), Kenji Kabashima[b], Takahiko Hara[c,f,m,2] (ID), and Hitoshi Okamura[a,l,2] (ID)

The epidermis is the outermost layer of the skin and the body's primary barrier to external pathogens; however, the early epidermal immune response remains to be mechanistically understood. We show that the chemokine CXCL14, produced by epidermal keratinocytes, exhibits robust circadian fluctuations and initiates innate immunity. Clearance of the skin pathogen *Staphylococcus aureus* in nocturnal mice was associated with CXCL14 expression, which was high during subjective daytime and low at night. In contrast, in marmosets, a diurnal primate, circadian CXCL14 expression was reversed. Rhythmically expressed CXCL14 binds to *S. aureus* DNA and induces inflammatory cytokine production by activating Toll-like receptor (TLR)9-dependent innate pathways in dendritic cells and macrophages underneath the epidermis. CXCL14 also promoted phagocytosis by macrophages in a TLR9-independent manner. These data indicate that circadian production of the epidermal chemokine CXCL14 rhythmically suppresses skin bacterial proliferation in mammals by activating the innate immune system.

epidermis | CXCL14 | circadian rhythms | *Staphylococcus aureus* | innate immunity

The skin is an organism's first line of defense against invading external pathogens. The outermost layer of the skin is called the epidermis; 95% of epidermal cells are epidermal keratinocytes, which proliferate in the basal layer of the epidermis and move to the upper layers as they mature and form cornified cells (1). Keratinocytes act as a passive barrier to mechanical injury and fluid loss and, along with epidermal Langerhans cells and dermal dendritic cells (DCs), as secretors of bioactive substances important in forming an immunological barrier (2–4). Although a number of studies have investigated the mechanisms underlying the cutaneous antibacterial immune response and skin innate immunity, factors involved in its early stages are not fully understood (5, 6).

Virtually all organisms—from bacteria to plants, invertebrates, and mammals—display biological rhythms controlled by the circadian clock, molecular machinery that operates in all cells (7–9). Circadian rhythms govern most behavioral, physiological, and metabolic functions (10). The organization of mammalian circadian rhythms is controlled by an autoregulatory transcription/posttranscription/translation-based feedback loop involving a set of clock genes (9, 11). The core clock genes are the positive transcription factors CLOCK and BMAL1, and the negative factors period (PER) and cryptochrome (CRY), which drive the expression of a large number of clock-controlled genes (CCGs) by binding to E-boxes. This core loop is reinforced by and embedded in other transcription feedback loops through CLOCK–BMAL1 activation of Rev-erbα and Rorα (12, 13). The molecular clock directs the expression of an estimated 10 to 20% of genes in all organs and tissues (14, 15). It is now clear that many highly differentiated tissues and cells in mammals express a common core clock oscillating system.

In the present study, we demonstrate the molecular mechanism by which a chemokine secreted in keratinocytes regulates skin *Staphylococcus aureus* invasion through Toll-like receptor (TLR)9-mediated innate immunity. By screening a circadian time-specific DNA microarray of WT and arrhythmic *Cry*-null mice, we identified a secretory molecule, the chemokine CXCL14, as a CCG prominently expressed in the mice epidermis. In the diurnal primate marmosets, circadian change of CXCL14 expression was observed, but the peak–trough profiles were reversed. CXCL14 is a small chemokine belonging to the major chemokine subgroup CXC, a subgroup that contains the sequence Cys-X-Cys at their N-terminal (16, 17). Chemokines are classified into two kinds, depending on their expression pattern: homeostatic or inflammatory (18). We show that the clearance of the skin pathogen *S. aureus* in nocturnal mice was associated with CXCL14 expression: high during subjective daytime and low at night. We further show that *S. aureus* DNA-induced induction of inflammatory cytokines was TLR9-dependent.

Significance

We found that among chemokine family members, only CXCL14 is abundantly produced in epidermal keratinocytes in a circadian rhythm-dependent manner. Whereas in nocturnal mice, CXCL14 expression was high during the day and low at night, in diurnal marmosets, expression was low during the daytime and high at night. Rhythmically expressed CXCL14 binds to bacterial DNA, leading to pathogen DNA-mediated Toll-like receptor 9 activation and promotion of phagocytosis, in this way serving to protect skin from overproliferation of the pathogen. We propose that during the resting period of animals, epidermis-derived CXCL14 acts on resident immune cells to regulate the skin's innate immunity.

Results

Identification of Circadian Clock-Regulated Genes in Mouse Keratinocytes. To elucidate the role of the circadian clock in epidermis-mediated immunity, we began the identification of CCGs in keratinocytes, since CCGs are key in understanding the role of circadian clocks in specific cells/tissues. For example, clock-controlled vasopressin and its receptors in the hypothalamic suprachiasmatic nucleus (19–21), where the mammalian master clock is located, play a key role in jetlag (22), while the activity of the longevity-related, NAD^+-dependent enzyme SIRT1 is dependent on NAD^+-regulating nicotinamide mononucleotide phosphoribosyltransferase, which is controlled by CLOCK–BMAL1 (23, 24). Thus, identification of CCGs in specific types of cells allows the physiological role of circadian clocks in living organisms to be uncovered.

Since mice are the most commonly used model of molecular and genetic physiology, C57BL/6 mice were used to identify bioactive molecules regulated by the circadian clock. However, the epidermal layer of mouse skin is very thin: mice epidermal keratinocytes consist of only one or two cell layers (25), from which it is very difficult to isolate mRNA for microarray analysis. Among the skin regions examined by paraffin sections stained with H&E, the footpads had the thickest epidermis (5 to 10 keratinocyte layers), which is exceptionally thick compared with other parts of the skin (Fig. 1 *A* and *B*). In the epidermis of footpads, keratinocytes make up more than 95% of total cells. We

isolated epidermal RNA samples with a laser microdissection (LMD) system (Leica LMD6000) in thick (30 μm) frozen cryostat sections. Six LMD samples were taken from each mouse (Fig. 1 *C* and *D*); four mice were sampled every 4 h in WT and *Cry*-null mouse groups (*n* = 4 for each genotype).

The CCGs in sampled microarrays were surveyed to identify those showing time-of-day variation. Among 2,540 genes showing one daily peak–trough profile, we focused on the timing of E-box–regulated genes (such as *Per1/2*) peaking at circadian time (CT)12−CT16, and Rorα/Rev-erbα–responsive element-regulated genes (such as *Bmal1*) peaking at CT20 to CT0 (*SI Appendix*, Fig. S1*A* and Dataset S1). Of particular interest were chemokines, since they have a variety of immune functions as local secretory molecules in innate immunity (6, 26), among which are circadian functions in the hematopoietic system (27). Microarray analysis of all known mouse chemokine genes in the skin epidermis (Fig. 1*E*) identified a gene probe (418457_s_at) with a signal peak at CT20/CT0 and a trough at CT12 in WT mice, but which was consistently low throughout the day in *Cry*-null mice. Moreover, the maximal expression level of this gene was the highest of all 39 chemokines expressed in the epidermis. This gene probe measures expression of *Cxcl14* mRNA.

Expression of CXCL14 in Mouse Keratinocytes Is Regulated by Circadian Rhythms. qRT-PCR analysis with gene-specific primers confirmed the circadian expression of the *Cxcl14* gene, with the peak at CT0 and the trough at CT8/12, which was
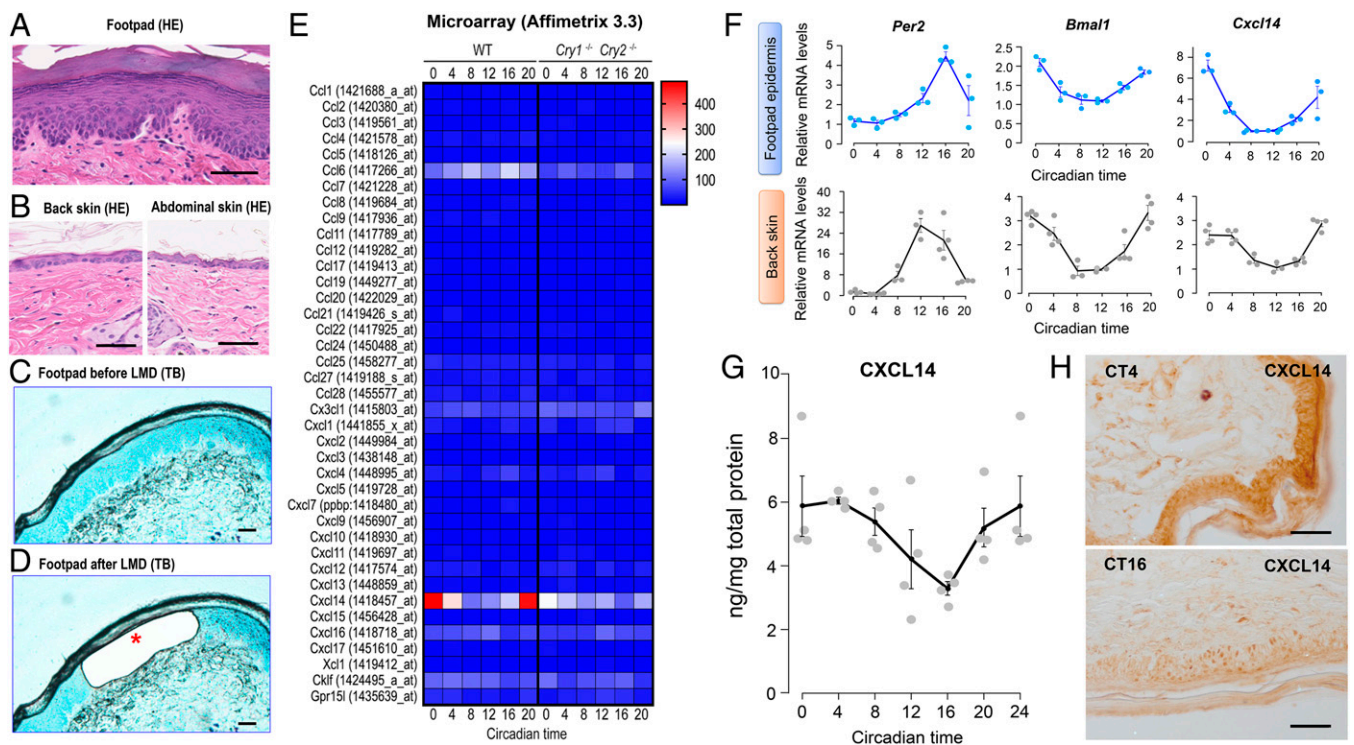

Fig. 1. Circadian expression of CXCL14 in skin epidermal keratinocytes. (*A* and *B*) Skin sections (5-μm-thick paraffin sections) from the footpad (*A*), back (*B*), and abdomen (*B*) stained with H&E. Note that stratified squamous epithelium was detected only in footpad epidermis. (Scale bars in *A* and *B*, 50 μm.) (*C* and *D*) An example of LMD applied to the epidermis of cryostat sections (30 μm thick) counterstained with Toluidine blue (TB). Before (*C*) and after (*D*) LMD (red asterisk). Note that only the epidermis was dissected out. (Scale bars in *C* and *D*, 50 μm.) (*E*) Twenty-four hour expression profiles of chemokine (CC, CXC, C, and CX3C) genes in skin footpad epidermis WT and *Cry*-null mice. The relative levels of each transcript, determined by DNA microarray analysis, are indicated by the color scale. For each transcript, values were normalized to the average expression level over the day in WT epidermis. The identity of each transcript is indicated by the Affymetrix probe used and the gene symbol (see also gene names shown in the *SI Appendix, Supplementary Text*). (*F*) qRT-PCR-verified 24 h expression profiles of *Per2*, *Bmal1*, and *Cxcl14* in WT and *Cry*-null footpad epidermis and back skin. Values are means ± SEM (*n* = 5 for footpad and *n* = 4 for back skin for each data point) normalized to expression of TATA-box binding protein-encoding gene. (*G*) Circadian expression profiles of CXCL14 protein of the skin by EIA (n = 4 for each data point). Note that CXCL14 peak–trough profiles from EIA were about 4 h after *Cxcl14* mRNA. (*H*) Differences in cellular expression of the CXCL14 protein in the footpad by immunohistochemistry. Note strong expression of CXCL14 in the majority of epidermal keratinocytes constituting stratified squamous epithelium, which are high at subjective morning (CT4) and low at subjective night (CT16). (Scale bars, 50 μm.) Data represent three or more independent experiments.

similar to *Bmal1* expression but the opposite of *Per2* expression in the epidermis. This circadian expression was also observed in samples of back skin, which contained all skin tissue layers (Fig. 1*F*).

Since many genes with circadian rhythms at the transcript level lose circadian expression at the protein level, we next examined whether the rhythmicity of *Cxcl14* gene expression was replicated in protein expression. Protein expression of CXCL14 was quantified by enzyme immunoassay (EIA). CXCL14 protein clearly demonstrated a robust circadian expression, and peak–trough profiles were about 4 h after *Cxcl14* mRNA (Fig. 1*G*).

To isolate CXCL14 expression at the cell level, in situ hybridization using isotope-labeled and digoxigenin-labeled CXCL14 probes was performed (*SI Appendix*, Fig. S1 *B* and *C*). Staining intensities of positive signals were higher in epidermal cells at CT4 than CT16. This was confirmed by immunohistochemistry in the footpad, where strong CXCL14-immunoreactivity in the majority of epidermal keratinocytes constituting stratified squamous cells at CT4 was evident (Fig. 1*H*). Consistent with RNA expression data, epidermal cell staining of CXCL14 was markedly suppressed at CT16. Similar circadian changes were observed in the thin epidermis from back skin (*SI Appendix*, Fig. S1*D*). These immunohistochemical and in situ hybridization findings agree with a circadian rhythm of CXCL14 at the protein and mRNA level.

CXCL14 Is a Target Gene of RORα. *Cxcl14* mRNA exhibited a similar peak–trough expression profile to Rorα/Rev-erbα–responsive element-regulated genes. Therefore, we examined whether the expression of *CXCL14* was induced by RORα in HaCaT cells, which are used as a model system for human keratinocytes. RORα was introduced in HaCaT cells via lentiviral infection with a PWPI-RORα vector, resulting in high RORα expression in HaCaT-PWPI-*RORα* (RORα) cells compared with noninfected HaCaT cells or PWPI empty vector-transduced HaCaT (empty) cells (Fig. 2*A*). qRT-PCR analysis showed that HaCaT-PWPI-*RORα* cells exhibited robust expression of *CXCL14* compared with noninfected HaCaT and empty HaCaT cells (Fig. 2*B*). The expression level of *BMAL1* was also increased in HaCaT-PWPI-*RORα* cells, but to a lower extent than *CXCL14* (Fig. 2*C*), suggesting that transcription of *CXCL14* strongly depends on RORα activity in HaCaT cells. We next searched for ROR response elements (ROREs) in the human *CXCL14* gene locus (± 2 kb from its transcription initiation site [TIS]) based on the RORE consensus sequence (WAWNTRGGTCA) and found one perfectly matched RORE site ~0.7 kb upstream of *CXCL14*'s TIS (Fig. 2*D*). Chromatin immunoprecipitation (ChIP) of the *CXCL14* locus using HaCaT-PWPI-RORα cells revealed that an anti-RORα antibody enriched the region 0.7 kb upstream of *CXCL14*'s TIS when compared with normal rabbit IgG (Fig. 2*E*). Enrichment with the anti-RORα antibody was not observed in the regions −1.3 kb, +1.3 kb, and +1.6 kb from *CXCL14*'s TIS (Fig. 2*E*), suggesting that RORα only interacted with the region −0.7 kb from the TIS of the *CXCL14* gene.

Consistent with this, cells overexpressing RORα displayed increased luciferase activity driven by the RORE located at −0.7 kb, but not by its mutated sequence (Fig. 2*F*). The increased luciferase activity in RORα cells was antagonized by REV-ERB (Fig. 2*F*). We found three RORE-like sequences (one or two bases mismatched): RORE-like 1 and 2 in the TIS region and RORE-like 3 +1.3 kb of the TIS in the human *CXCL14* gene (*SI Appendix*, Fig. S2*A*). RORα did not increase the reporter activities driven by RORE-like 1 and 2 (*SI Appendix*, Fig. S2 *B* and *C*), whereas it moderately increased luciferase activity driven by RORE-like 3 (*SI Appendix*, Fig. S2*D*). These results suggest that the expression of *CXCL14* is controlled by the RORα/REV-ERB system, mainly through the RORE located 0.7 kb upstream of the TIS region.

Antibacterial Function of CXCL14 in the Skin. Interestingly, CXCL14 is known to be constitutively expressed in epithelial tissues at high levels in the skin, gastrointestinal, and urinary tracts (17); in primate tastebuds, *CXCL14* is the most abundantly expressed gene (28). In contrast to inflammatory chemokines such as CCL20, the expression of CXCL14 is suppressed by proinflammatory stimuli, such as interleukin (IL)-1, tumor necrosis factor (TNF)-α, and lipopolysaccharide in human keratinocytes (29, 30). Using bone marrow-derived DCs (BMDCs), Tanegashima et al. (26) found that CXCL14 binds to bacterial CpG DNA with high affinity and up-regulates cell uptake, with a robust induction of TLR9-dependent production of inflammatory cytokines (26). Although these findings suggest that CXCL14 has a role in immunity, they remain to be confirmed, meaning the mechanism by which CXCL14 functions in antibacterial immunity is not fully elucidated.

To clarify the role of circadian expression of epidermal CXCL14 in skin immunity, we focused on *S. aureus*, since it is a particularly prevalent infection in humans: around 30 to 100% of the human population are long-term carriers of *S. aureus* (31), which can be found as part of the normal skin flora and as a pathogen. In 2017, an estimated 119,247 *S. aureus* bloodstream infections with 19,832 associated deaths occurred (32). In addition, the widespread emergence of nosocomial and community-acquired methicillin-resistant (CA-MRSA) strains is a major health problem: mortality resulting from MRSA infections is comparable to mortality resulting from AIDS, tuberculosis, and viral hepatitis combined (33). The fact that most systemic sequelae caused by *S. aureus* originate from skin infections necessitates an in-depth understanding of the cutaneous antibacterial immune response.

Virtually all processes of the immune response (innate and adaptive) oscillate in a circadian manner (34–36). Since CXCL14-expressing keratinocytes lie in the front line of bacterial invasion, we focused our attention on the early stages of pathogen exposure in the skin. Time-of-day–dependent differences in bacterial proliferation were examined in the skin in young-adult mice (6 wk of age). Intracutaneous injection of *S. aureus* (1×10^7 colony-forming units [CFUs per ear) was performed during the day (Zeitgeber time [ZT] 4; 4 h after light-onset) or at night (ZT16; 4 h after light-offset). Bacterial proliferation in the injected skin 6 h after injection (ZT10 and ZT20) was significantly higher at night than in the day ($P < 0.01$) (Fig. 3*A*). The same experiment was performed in adult mice (12 wk old, by which time immunity is firmly established) after a day of transition to constant dark conditions to eliminate the effect of environmental light–dark cycles. In these mice, similar circadian rhythms of bacterial proliferation at injected skin sites were observed (significantly higher at night than in the day, $P < 0.05$) (Fig. 3*B*).

We next investigated whether bacterial proliferation was affected in the presence of CXCL14. Compared with adult WT mice, adult *Cxcl14*-deleted mice ($Cxcl14^{-/-}$) had higher levels of bacterial proliferation when injected with *S. aureus* during the day ($P < 0.01$ in Fig. 3*C*, and $P < 0.05$ in *SI Appendix*, Fig. S3*A*). Moreover, CXCL14-overexpressing transgenic (Tg) mice had lower levels of bacterial proliferation ($P < 0.05$) (Fig. 3*D*), suggesting that CXCL14 inhibits bacterial proliferation. Since the nighttime increase in bacterial proliferation
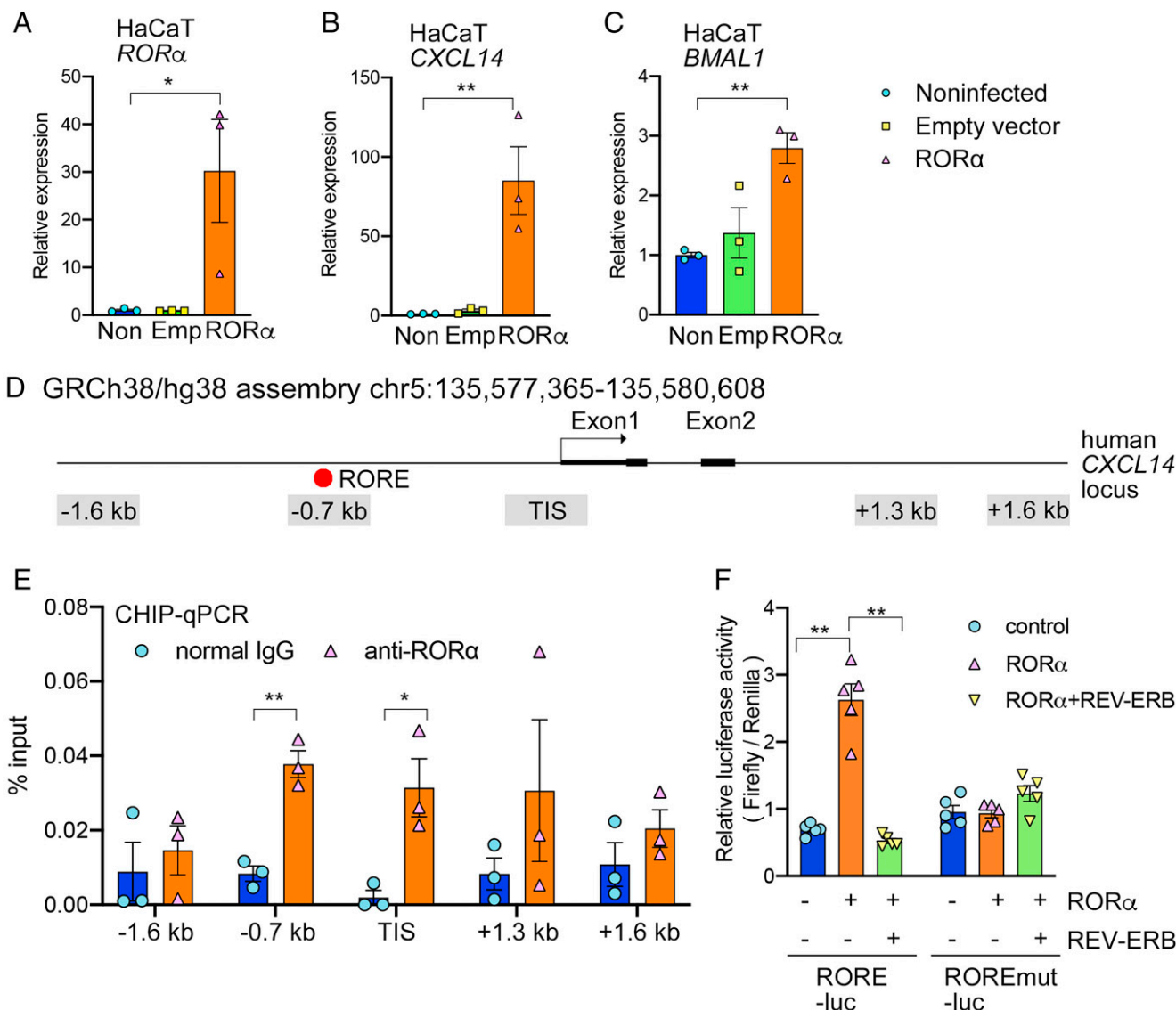
Fig. 2. CXCL14 is a target gene of RORα. (*A*–*C*) qRT-PCR analysis of human keratinocyte-derived HaCaT cells stably transduced with a PWPI (Empty; Emp) or PWPI-RORα (RORα) lentiviral vector. The relative expression levels of *RORα* (*A*), *CXCL14* (*B*), and *BMAL1* (*C*) are shown. The expression level of noninfected (Non) HaCaT cells were adjusted to 1.0, and results were expressed relative to noninfected cells. (*D*) Genomic structure of the *CXCL14* locus in human chromosome 5. The red circle indicates the RORE consensus sequence. Gray bars represent the regions amplified by ChIP-qPCR. (*E*) ChIP-qPCR analysis of the HaCaT-PWPI-*RORα* cell line using normal rabbit IgG and a rabbit anti-RORα antibody. (*F*) Luciferase activity driven by RORE. Three tandem repeats of 21-bp sequences around RORE at the −0.7-kb region and its mutant version were inserted upstream of the firefly luciferase reporter gene. These luciferase constructs and pRL-CMV *Renilla* luciferase reporters were transfected into mouse embryonic fibroblasts with empty pCMV-SPORT6 vector (control), pCMV-SPORT6-*Rorα*, or pCMV-SPORT6-*Rorα* + pCMV-SPORT6-*Rev-erbα* to measure dual luciferase activities. The activities of firefly luciferase were normalized to *Renilla* luciferase. In *A*–*C*, statistical analyses were done using a one-way ANOVA with Sidak's multiple comparisons versus noninfected sample for three independent experiments. (*$P < 0.05$, **$P < 0.01$, otherwise not significant). In *E*, the two-tailed, unpaired Student's *t* test was used (*$P < 0.05$, **$P < 0.01$, otherwise not significant) using the value of three independent experiments. In *F*, statistical analyses were done using a one-way ANOVA with Sidak's multiple comparisons (*$P < 0.05$, **$P < 0.01$, otherwise not significant) using technical replicates ($n = 5$); mean ± SEM is shown.

did not occur in *Cxcl14*$^{-/-}$ mice (Fig. 3*E*), it appears that a daytime increase of CXCL14 in the skin suppresses bacterial proliferation. Gene-expression profiles of infected ears from WT and *Cxcl14*$^{-/-}$ mice suggest that the expression of inflammatory genes was suppressed in infected ears from *Cxcl14*$^{-/-}$ mice (*SI Appendix*, Fig. S3*B*). qRT-PCR analysis showed that 3 h after infection, expression of inflammatory cytokine genes— such as *Il1b*, *Cxcl2*, and *Ccl3*—was suppressed in the ears of *Cxcl14*$^{-/-}$ mice infected during the day (Fig. 3 *F*–*H*). *S. aureus* infection was quantified by *S. aureus* rRNA and was comparable between WT and *Cxcl14*$^{-/-}$ mice at this time (Fig. 3*I*). These results suggest that CXCL14 is involved in activation of inflammatory responses to *S. aureus* infection, resulting in suppression of bacterial proliferation.

CXCL14 Recognizes *S. aureus* DNA to Activate the TLR9 Pathway. Previously, we demonstrated that CXCL14 binds to bacterial CpG DNA and carries it to endosomes in BMDCs, which activates TLR9-mediated innate immunity (26). To find out whether these molecular events occur during *S. aureus* infection, we carried out a plate-based binding assay for CXCL14 (37). qPCR analysis of *S. aureus* DNA indicated that *S. aureus* DNA bound to a CXCL14-coated plate, but not to a non-coated plate (Fig. 4*A*). In the presence of ODN2395, a competitive CpG oligonucleotide (ODN) with high affinity to CXCL14, binding of *S. aureus* DNA no longer occurred (Fig. 4*A*). We also analyzed the binding of *S. aureus* DNA to mouse macrophage-derived RAW264.7 cells in the presence or absence of CXCL14 (Fig. 4*B*). qPCR analysis suggested that cell surface
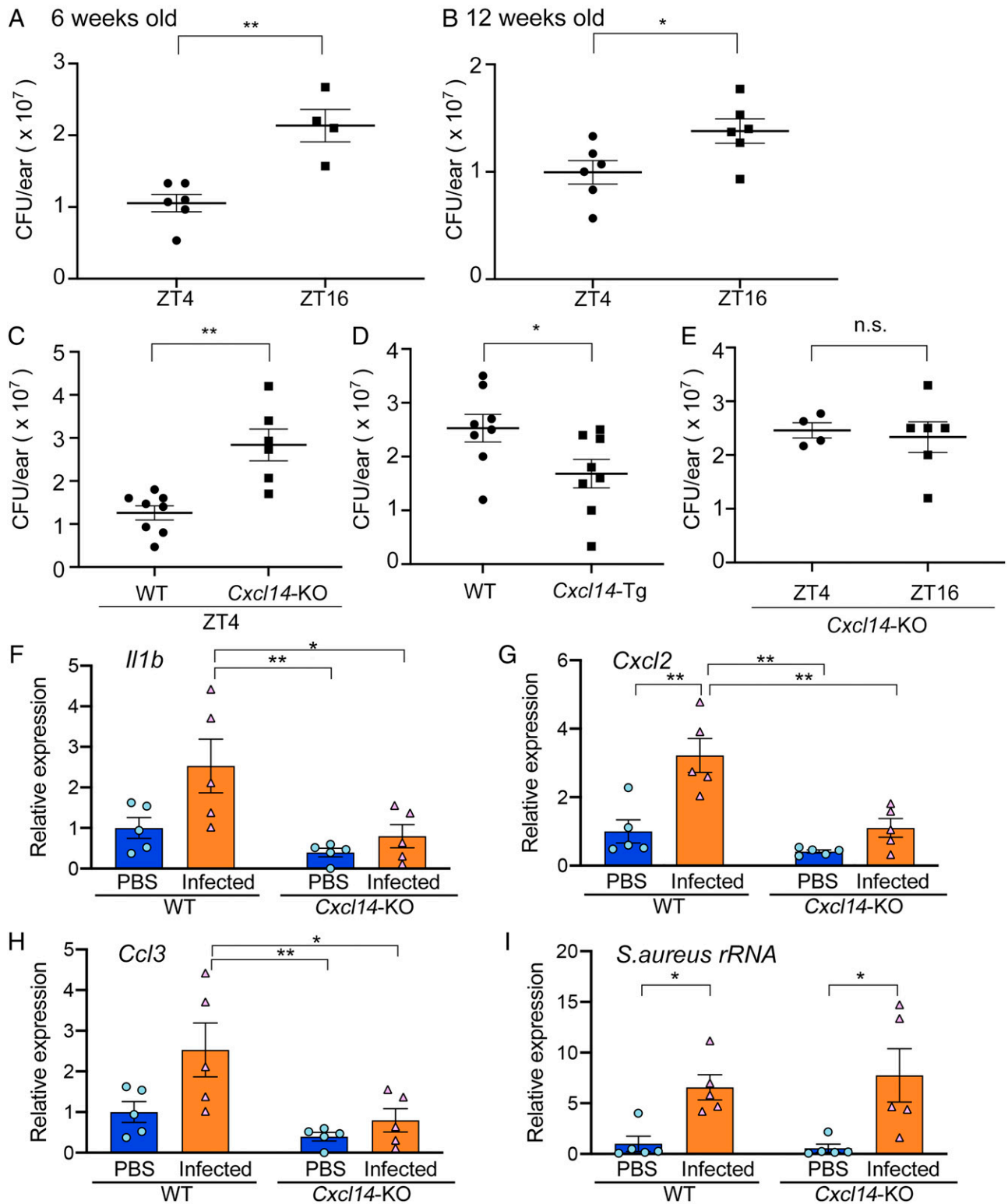
Fig. 3. Effect of circadian time on bacterial proliferation in WT and *Cxcl14*$^{-/-}$ mice. (*A*) Time-of-day–dependent differences in bacterial proliferation in young-adult (6-wk-old) male C57BL/6 mice. *S. aureus* (1×10^7 CFUs per ear) was injected intracutaneously to the ear skin at ZT4 or ZT16, and its proliferation was measured 6 h after injection (ZT10 and ZT22). **$P < 0.01$; $n = 4 - 6$ per group; statistical analysis was performed using the Student's two-tailed unpaired *t* test. (*B*) The same experiment as *A* was performed in 12-wk-old adult male mice housed with a day of transition to constant dark conditions to eliminate the effect of environmental light/dark cycles ($n = 6$ per group). *$P < 0.05$; Student's two tailed unpaired t test. (*C*) Deletion of *Cxcl14* abolished the time-dependent suppression of bacterial proliferation in 14- to 15-wk-old female mice. *CXCL14*$^{-/-}$ mice were infected intradermally with *S. aureus* (1×10^7 CFUs per ear) at ZT4, as were WT mice in *A* ($n = 6 - 8$). **$P < 0.01$; Student's two tailed unpaired t test. (*D*) Overexpression of CXCL14 in 13-wk-old *CXCL14*-Tg male mice suppressed bacterial proliferation at ZT16 ($n = 8$ per group). *$P < 0.05$; Student's two tailed unpaired t test. (*E*) Bacterial load of ears was comparable between ZT4 and ZT16 in 12-wk-old *Cxcl14*$^{-/-}$ male mice ($n = 4 - 6$). n.s.: not significant according to the Student's two-tailed unpaired *t* test. (*F–I*) Expression profiles of cytokine genes [*Il1b* (*F*), *Cxcl2* (*G*), *Ccl3* (*H*) compared with rRNA gene of *S. aureus* (*I*)]. Samples were collected from the injected dermis 3 h after infection with *S. aureus* at ZT4 in 12-wk-old WT and *Cxcl14*$^{-/-}$ female mice and analyzed with qRT-PCR ($n = 5$). Note that expression of these genes was increased in WT mice, but significantly reduced in *Cxcl14*$^{-/-}$ mice. In *F–I*, statistical analyses were applied using a two-way ANOVA with Sidak's multiple comparisons (*$P < 0.05$, **$P < 0.01$, otherwise not significant). Individual points represent mean values of both ears from individual mice (*A–E*); mean ± SEM is shown.
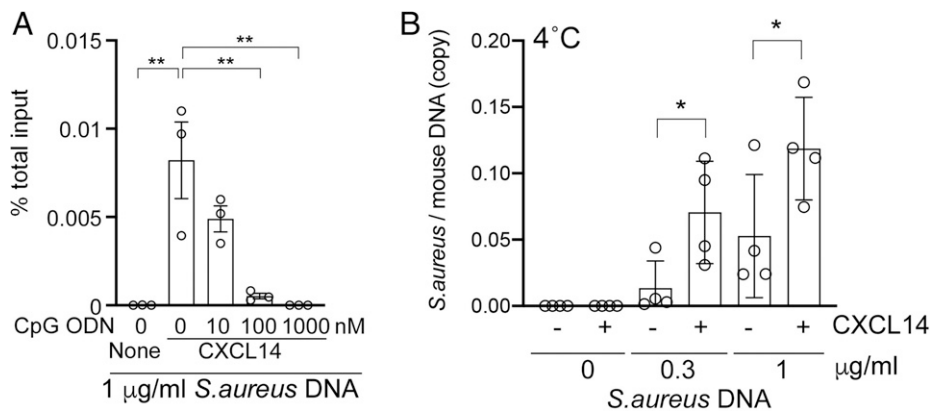
Fig. 4. Enhanced binding of the *S. aureus* DNA/CXCL14 complex to RAW264.7 cells. (*A*) A multiwell, plate-based binding assay was used to immobilize CXCL14 by incubation. Coated wells had *S. aureus* DNA (1 μg/mL) added, in combination with increasing amounts of ODN2395 for 1 h at room temperature. Wells without CXCL14 coating were used as controls (None). The amount of bound *S. aureus* DNA was measured by quantitative PCR using *S. aureus* Nuc primers. The mean of triplicate measures of bound/input DNA are shown with SEM. The same set of experiments was repeated, and similar results were obtained. Statistical analyses were done using a one-way ANOVA with Sidak's multiple comparisons (*$P < 0.05$, **$P < 0.01$, otherwise not significant) using technical triplicates. (*B*) RAW264.7 cells in 24-well plates were treated with *S. aureus* DNA in the presence or absence of 300 nM CXCL14 at 4 °C for 1 h. Thereafter, genomic DNA was isolated, and the copy number ratio of *S. aureus* DNA to mouse genome DNA was determined by qPCR using primer pairs of *S. aureus* Nuc and mouse rRNA. Statistical analyses were done using a one-way ANOVA with Sidak's multiple comparisons between values with and without CXCL14 (*$P < 0.05$, **$P < 0.01$, otherwise not significant). Values from four independent experiments are shown.

binding of *S. aureus* DNA to RAW264.7 was increased in the presence of CXCL14. A previous report demonstrated that CXCL14 enhances the binding of CpG ODN to RAW264.7 cells (37); therefore, these results indicate that *S. aureus* DNA forms a complex with CXCL14 and enhances its binding to the receptor. Consistent with this result, CXCL14 augmented TNF-α and Cxcl2 responses after treatment with *S. aureus* DNA (Fig. 5 *A* and *B*). The enhanced TNF-α response to bacterial DNA depended on the species of bacterial DNA, since CXCL14 did not increase (but rather suppressed) the TNF-α response to *Eschelichia coli* DNA in RAW264.7 cells (*SI Appendix*, Fig. S4A). mRNA expression of *Il1b* and *Ccl3* was also up-regulated in the presence of CXCL14 (Fig. 5 *C* and *D*), suggesting that *CXCL14* activates inflammatory responses to *S. aureus*. The induction of the inflammatory response was prevented by *Tlr9* knockout (Fig. 5 *A*−*D*), and up-regulation of *Il1b*, *Ccl3*, and *Cxcl2* expression was not observed in *S. aureus*-infected skin samples of *Cxcl14*⁻/⁻ mice (Fig. 3 *F*−*I*). These data suggest that CXCL14 and bacterial CpG DNA synergistically activate TLR9-dependent innate pathways.

To determine the species-specificity of bacterial DNA, and whether TLR9 dependency is maintained in DCs, we investigated the expression of *Cxcl2* and *Il1b* in BMDCs. It is known that Cxcl2 and IL-1β are induced after *S. aureus* infection in the skin (5). CXCL14 enhanced the induction of these cytokine genes by *S. aureus* DNA in BMDCs from WT mice, but not from *Tlr9*⁻/⁻ mice (Fig. 5 *E* and *F*). To examine whether the TLR9 pathway is also important for skin infection of *S. aureus* in vivo, we injected *S. aureus* into the ear skin of WT and *Tlr9*⁻/⁻ mice. Levels of bacterial proliferation in *Tlr9*⁻/⁻ mice were significantly higher ($P < 0.05$) than in WT mice (Fig. 5G). Moreover, augmentation of *S. aureus* proliferation by the application of the TLR9 antagonist ODN2088 was not observed in *Cxcl14*⁻/⁻ mice (Fig. 5H). These findings strongly suggest that CXCL14 strengthens *S. aureus*-induced immunity via the TLR9 pathway. Of note, CXCL14 also appears to elicit a TLR9-indendent defense against *S. aureus*, since exogenously expressed CXCL14 in *Tlr9*⁻/⁻ mice suppressed *S. aureus* proliferation (*SI Appendix*, Fig. S4B). In a previous report, rhythmically expressing TLR9 in the spleen contributed to the severity of sepsis in a cecal ligation and puncture model (38). However,

we did not observe prominent rhythms in *Tlr9* expression in the skin.

CXCL14 Enhances Phagocytosis of *S. aureus* Particles. We also examined the effect of CXCL14 on phagocytosis, the initial state of innate immunity, in the presence or absence of *S. aureus* DNA. CXCL14 alone increased phagocytosis in pHrodo-labeled *S. aureus* particles in peritoneal macrophages and RAW264.7 cells (*SI Appendix*, Fig. S5). Surprisingly, *Tlr9*⁻/⁻ peritoneal macrophages and *Tlr9*⁻/⁻ RAW264.7 cells also exhibited up-regulation of phagocytosis by CXCL14. These findings suggest that CXCL14 facilitates phagocytic activity in a TLR9-independent manner.

Reversed Circadian CXCL14 Expression in the Epidermis of Diurnal Primate Marmosets. Beyond the cellular level, tissue and in vivo findings suggest that daytime-expressed CXCL14 in keratinocytes plays an important role in innate immunity in skin DCs: in humans, high CXCL14 levels were observed in the epidermis (29, 39). To translate our keratinocyte results to human skin diseases, our findings were confirmed in nonhuman primates. We selected the diurnal common marmoset (*Callithrix jacchus*), a small, New World monkey whose genome was the first totally sequenced in primates (40). Compared with the C57BL/6 mouse strain, which show nocturnality, marmosets show complete diurnality in locomotor activity (41) and core body temperature (Fig. 6A). In marmosets, circadian CXCL14 expression was reversed compared with mice: CXCL14 expression was low during the daytime and high at nighttime (Fig. 6 *B* and *C*). These data indicate that circadian production of epidermal CXCL14 may act via a noncanonical mechanism to rhythmically regulate skin bacterial proliferation in mammals by activating the innate immune system.

Discussion

In this study, we revealed that the chemokine CXCL14 is produced by keratinocytes in a circadian rhythm-dependent manner and protects skin from overproliferation of *S. aureus* during the early phase of resting (Fig. 6D). CXCL14 is a secretory protein known to accumulate in the extracellular matrix due to its heparin-binding properties (42). CXCL14 directly binds to
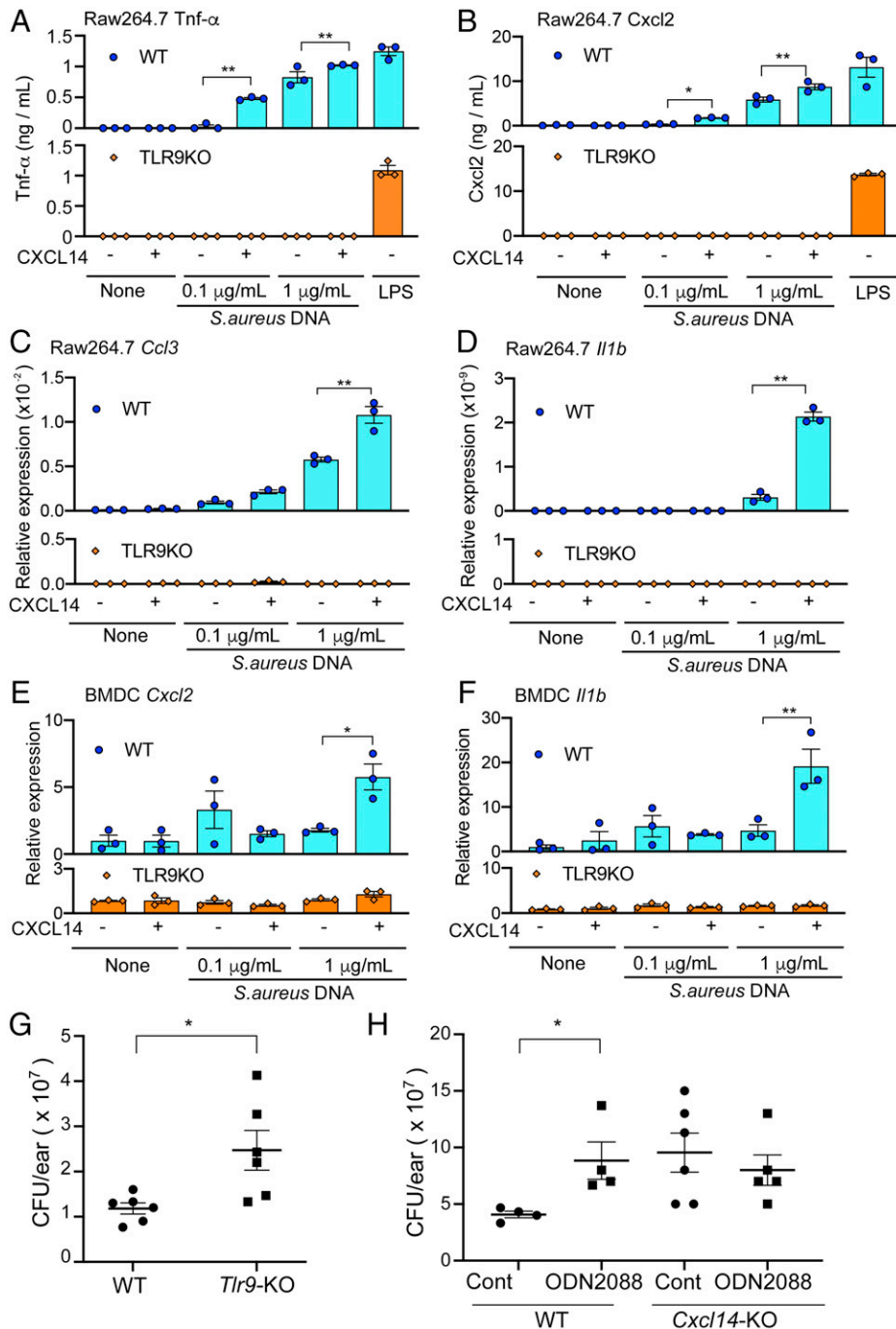
Fig. 5. TLR9-dependent Cxcl14 action on *S. aureus* infection. (*A* and *B*) ELISA analysis of WT and *Tlr9*$^{-/-}$ RAW264.7 cells treated with CXCL14 and *S. aureus* DNA. These cells were treated with 0, 0.1, and 1 μg/mL of *S. aureus* DNA in the presence or absence of 300 nM CXCL14 for 6 h. Culture supernatant was subjected to ELISA analysis for TNF-α (*A*) or Cxcl2 (*B*). (*C−F*) qRT-PCR analysis of WT RAW264.7 cells (*C* and *D*), *Tlr9*$^{-/-}$ RAW264.7 cells (*C* and *D*), WT BMDCs (*E* and *F*), and *Tlr9*$^{-/-}$ BMDCs (*E* and *F*) treated with CXCL14 and 0, 0.1, and 1 μg/mL of *S. aureus* DNA in the presence or absence of 300 nM CXCL14 for 6 h, as shown in *A* and *B*. RNA was extracted to make cDNA for qRT-PCR; *β-actin* was used as an internal control. The mean expression ± SEM of *Ccl3* (*C*), *Il1b* (*D* and *F*), and *Cxcl2* (*E*) relative to the nontreated control (adjusted to 1) is shown. In *A−F*, statistical analyses were carried out using a two-way ANOVA with Sidak's multiple-comparison tests on the WT group with and without the addition of CXCL14 (*$P < 0.05$, **$P < 0.01$, otherwise not significant; n = 3). (*G*) Ears of 9-wk-old WT or *Tlr9*$^{-/-}$ male mice were inoculated intracutaneously with *S. aureus* (1×10^7 CFUs per ear) at ZT4. The titer of *S. aureus* infection was determined 6 h after inoculation (n = 6 at each group). Statistical analysis was performed using the Student's two-tailed, unpaired *t* test (*$P < 0.05$). (*H*) Ears of 12-wk-old WT or *Cxcl14*$^{-/-}$ male mice were inoculated intracutaneously with *S. aureus* (1×10^7 CFUs per ear) with the TLR9 antagonist oligonucleotide, ODN2088, or a negative control oligonucleotide (Cont) at ZT4 (n = 4 to 6 per group). The titer of *S. aureus* infection was determined 24 h after inoculation. Statistical analysis was applied using the Kruskal–Wallis test with Dunn's multiple comparisons (*$P < 0.05$, otherwise not significant). In *G* and *H*, individual points represent mean values of both ears from individual mice; mean ± SEM is shown.

S. aureus DNA and transports it into DCs/macrophages residing in dermal layers, thereby inducing TLR9-dependent cytokine production. We also found that CXCL14 promotes phagocytosis of *S. aureus* by macrophages in a TLR9-independent manner. This is a unique innate immune system response that involves

circadian rhythms in the epithelial cells interacting with DCs/macrophages in the initial stages of bacterial infection.

The circadian changes of CXCL14 expression in the epidermis observed in the present study are in agreement with identification of clock-regulated chemokine genes in other tissues.
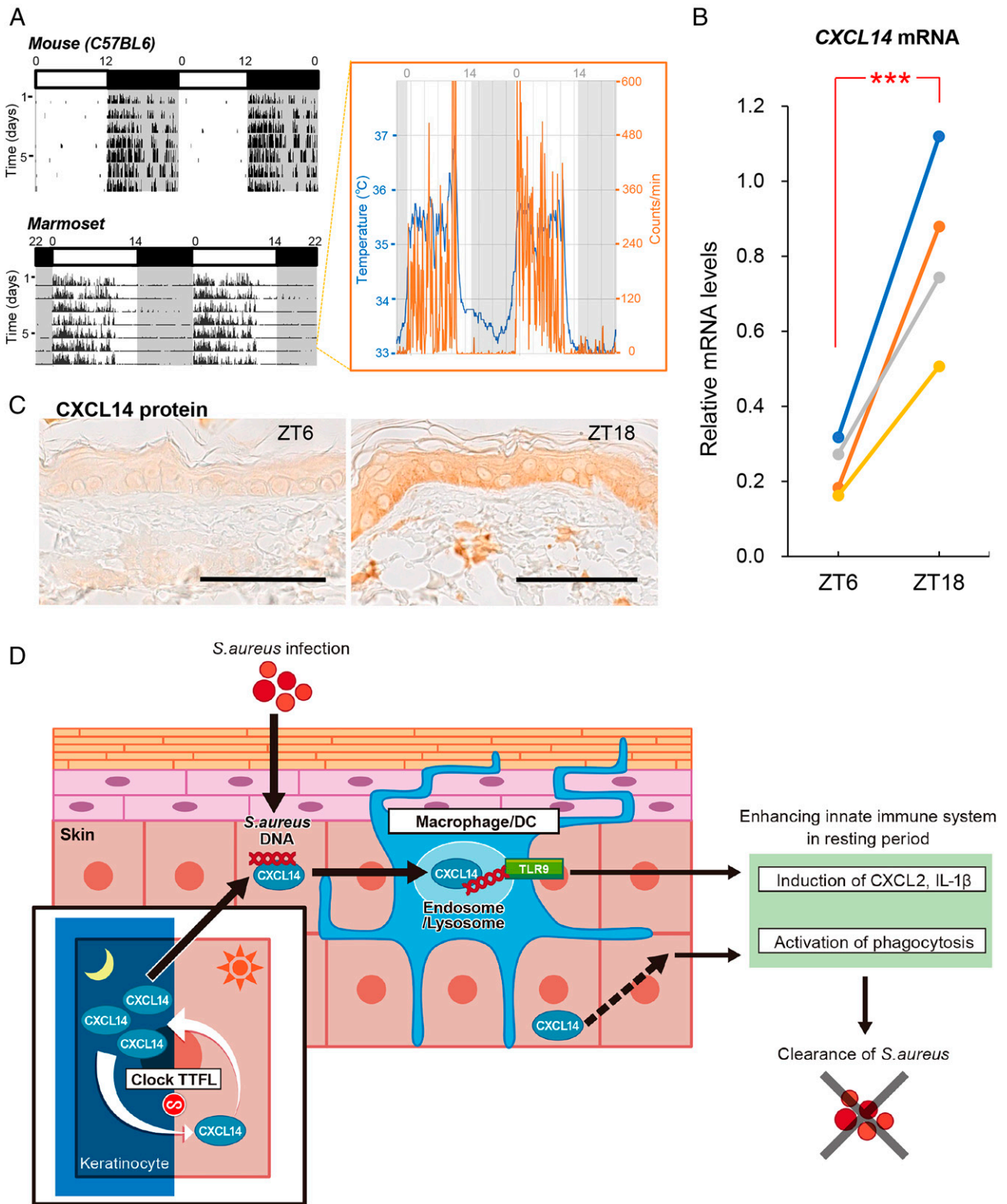
Fig. 6. Reversed rhythmic expression of Cxcl14 in diurnal marmosets. (*A*) Comparative locomotor activity rhythms of mice (*Mus musculus*, C57BL/6) and marmosets (*C. jacchus*) in light/dark cycles shown in representative double-plotted actograms. Daily variation of locomotion (orange line; counts per minute) and body temperature (blue line; mean temperature per minute) in marmosets are also shown for 2 d (sixth and seventh day). Light-on time is shown with a white background area, and light-off with a gray background area. Note that marmosets are diurnal, but mice are nocturnal. (Scale bars, 50 μm.) (*B*) Pairwise comparisons of *Cxcl14* mRNA in the epidermis at ZT6 and at ZT18. qPCR analysis for two male (blue and gray) and two female (dark orange and light orange) marmosets. Note the two- to fourfold change in *Cxcl14* mRNA levels. ***$P < 0.001$, Student's paired *t* test in marmoset skin. (*C*) Immunohistochemistry of CXCL14 protein in marmoset skin at ZT6 and ZT18. Note CXCL14 protein is strongly expressed in epidermal cells at night. (Scale bars, 50 mm.) (*D*) Schematic model of circadian clock-mediated clearance of *S. aureus* by CXCL14 in the epidermis of marmosets. Transcription–translation feedback loop (TTFL) of clock genes in keratinocytes regulates circadian expression of the *Cxcl14* gene in epidermal keratinocytes. Keratinocytes produce and secrete CXCL14 into the extracellular matrix during the resting period, which for diurnal animals is at night. When *S. aureus* invades skin keratinocytes, CXCL14 binds to degraded CpG DNAs and transports them into DCs/macrophages. Subsequently, TLR9 in the endosome/lysosome is activated, and cytokines including CXCL2 and IL-1β are induced. In addition to the TLR9 pathway, CXCL14 enhances phagocytotic activity of DCs/macrophages. CXCL14 therefore serves in the innate immune defense against *S. aureus*.

Gibbs et al. (43) previously reported that CXCL5 expression was regulated in a circadian rhythm-dependent manner and was involved in neutrophil recruitment in the lungs. In addition, release of hematopoietic stem cells from bone marrow was regulated by a reduction of CXCL12 levels during the resting period (i.e., subjective nighttime) (27).

Previous studies indicate that CXCL14 is involved in antibacterial immunity (29, 44). By using a respiratory infection model with intranasally administered bacteria, Dai et al. (44) demonstrated that CXCL14-knockout mice had decreased clearance of *Streptococcus pneumoniae*, suggesting that CXCL14 in the respiratory epithelium was involved in respiratory infection response. However, the mechanism by which CXCL14 affects immunity remains unresolved. Molecular structural analysis suggests that CXCL14 is a broad-spectrum antimicrobial peptide: the high proportion of cationic amino acids in the C terminus of CXCL14 may allow it to bind to, and destroy, the negatively charged phospholipids in bacterial membranes (44). Indeed, exposing cultured bacteria to CXCL14 inhibits their proliferation in both gram-positive and gram-negative bacteria (44), although in this case, the effective medium concentration (EC_{50}) was extraordinarily high (*E. coli* 0.32 μM, *S. aureus* 5.17 μM, *S. pneumoniae* ~0.5 μM EC_{50}, respectively) (44), which may not be physiologically relevant. CXCL14 also shows weak chemotaxic activity on activated macrophages, immature DCs, and natural killer cells (16).

Since CXCL14 levels in the epidermis are maximal during the early resting period, mammals are highly dependent on this system for skin protection from overproliferation of *S. aureus*. Therefore, CXCL14 could be utilized as a barrier against other pathogen/damage-associated molecular patterns; elucidation of such targets would help better understand skin immunosurveillance.

Materials and Methods

Mice. $Cxcl14^{-/-}$ male and $Cxcl14^{+/-}$ female mice on a C57BL/6 background were crossed to produce $Cxcl14^{+/-}$ and $Cxcl14^{-/-}$ mice, as previously described (45). $Tlr9^{-/-}$ mice (46) were obtained from Oriental Bioservice, Inc. and mated to produce $Tlr9^{-/-}$ mice. CXCL14-transgenic mice (47) were mated with $Tlr9^{-/-}$ mice or C57BL/6 mice (Nihon SLC). All mice were housed in a pathogen-free animal facility under a 12-h light/dark cycle. Genotyped, 6- to 15-wk-old mice and age- and gender-matched C57BL/6 controls were used for experiments.

The generation and breeding of *Cry*-null mice has been described previously (48–50). Before experiments, we housed both WT and *Cry*-null mice for at least 2 wk in a 12-h light/dark cycle (0600 hours, light on/1800 hours, light off) to synchronize (entrain) the circadian clock to the ambient light/dark cycle in a constant room temperature (22 ± 2 °C). Locomotor activity was detected by infrared sensors, and data were analyzed with Clocklab software (ActiMetrics). ZT was defined as ZT0 when the light was switched on. To eliminate external light, we transferred the mice into constant darkness 2 d before being killed; mice were killed every 4 h beginning at CT0, which represents subjective dawn. To eliminate gender- and age-related variations, we routinely used 12- to 16-wk-old male mice.

All experimental procedures were preapproved by the Animal Experimentation Committee at Kyoto University and the Ethical Committee of Tokyo Metropolitan Institute of Medical Science.

Marmosets. The marmosets used for the experiment were two males and two females aged from 0.9 to 4.1 y old. Marmosets were housed under cyclic light/dark conditions (14-h light period and 10-h dark period; 0600 hours, light on/2000 hours, light off) at a constant room temperature (28 ± 0.8 °C). Light-on time was defined to ZT0. At ZT6 (6 h after onset of light) and ZT18 (2 h after lights off), marmoset skin specimens (5-mm squares) were obtained from the dorsal skin under general anesthesia (ketamine 30 mg/kg; atropine 0.05 mg/kg, intramuscular injection). The surgery was performed at intervals of 2 wk or more to eliminate the effects of changes in general condition due to the operation.

Specimens were immediately frozen with dry ice or fixed with 4% paraformaldehyde in 0.1 M phosphate buffer. To detect circadian rhythms of sleep/wake cycles of marmosets, in some cases we implanted a small body temperature/activity frequency-measuring device (Kissei Comtech Nanotag) into the peritoneal cavity under general anesthesia by inhalation of isoflurane and measured both core body temperature and activity frequency every 5 min. All animal experimental protocols for marmosets were in accordance with the guidelines for animal experiments approved by the Animal Ethics Committee at Kyoto University.

Microarray Analysis. For circadian analysis of epidermal expressions, animals (12 WT mice, 12 *Cry*-null mice) were killed by cervical dislocation under a red safety light at the indicated time points in constant dark condition. Total RNA was prepared from two pools of LMD-sampled footpad epidermis ($n = 2$) at each time point to duplicate our observations on two independent arrays. Total RNA was isolated with the RNeasy mini kit (Qiagen), and the integrity was assessed by analyzing aliquots on an Agilent 2100 Bioanalyzer (Agilent Technologies). cDNA synthesis and cRNA labeling were performed using the One-Cycle Target Labeling and Control Reagents Kit (Affymetrix), and subsequent hybridization was performed with GeneChip Mouse Genome 430 2.0 array (Affymetrix) according to the manufacturer's protocol. For data analysis, we used the robust multiarray analysis (RMA) expression measure 48, which represents the log-transformed value of (background-corrected and normalized) intensities of the GeneChips. The RMA measures were computed using the R package program, which is freely available on the website (www.bioconductor.org). The value of each time point was expressed as a mean of two independent chips, which yielded equivalent results. For each transcript, values were normalized to the average expression level over the day in the WT skin epidermis.

For analysis of gene expression changed by *S. aureus* infection, infected and control ears from WT or $Cxcl14^{-/-}$ mice were homogenized in Isogen (Nippongene), and total RNA was isolated. Integrity of each RNA preparation was verified using a Bioanalyzer (Agilent Technologies). Cy3-labeled cRNA probes were synthesized and hybridized with Whole Mouse Genome Microarray 4 × 44K v2 (Agilent Technologies) according to the manufacturer's instructions.

Complete microarray datasets are available under accession numbers GSE174155 and GSE164899 (Gene Expression Omnibus: https://www.ncbi.nlm.nih.gov/geo/).

ChIP Assay. ChIP assays were performed using a rabbit anti-RORα antibody (Thermo Fisher Scientific) or normal rabbit IgG (Wako), as previously described (51). We used 5 μL of protein A Sepharose (GE Healthcare) and 1 μg of antibody in each ChIP reaction. IP or intact chromatin DNA fractions were digested with proteinase K (Wako) followed by gel filtration. The ratio of IP DNA to total chromatin DNA was determined by qPCR using specific primers for the *CXCL14* gene (*SI Appendix*, Table S1).

Bacteria. An *S. aureus* strain (ATCC25923) was purchased from ATCC. Bacteria were grown to midlog phase in Luria-Bertani (LB) broth, washed, and resuspended in PBS. Bacterial concentrations were estimated with a spectrophotometer by determining the optical density at 600 nm (OD_{600}). CFUs were verified by plating dilutions of the inoculum onto LB agar overnight at 37 °C.

For *S. aureus* DNA, overnight bacterial culture was pelleted to be treated with lysostaphin (SAE0091, Sigma) followed by proteinase K (Wako) treatment. Bacterial lysate was extracted by phenol and chloroform to purify DNA. After ethanol precipitation, DNA was dissolved and treated with RNase A (Wako). The DNA was further purified by phenol and chloroform extraction followed by ethanol precipitation.

Mouse Model of *S. aureus* Cutaneous Infection. The epicutaneous *S. aureus* exposure model is commonly used for evaluating epidermal protein on the infection of *S. aureus* in the epidermis (52). However, the epidermis is covered by the thick stratum corneum that blocks the penetration of bacteria to the deeper layer of the skin. Since the purpose of this study is to examine local and short-term actions of CXCL14 against bacterial proliferation inside the skin, we adopted an intradermal *S. aureus* injection model (6).

For the in vivo infection experiments of WT and $Cxcl14^{-/-}$ mice, 1×10^7 CFUs of *S. aureus* were injected intradermally in a small volume of PBS (10 μL) into the pinnae of each ear using a 30-G insulin syringe (Nippon Becton Dickinson) under anesthesia with a ketamine/xylazine mixture (Ketamine 50 mg/kg by

weight and xylasine 20 mg/kg by weight). For the TLR9 antagonist injection, 0.2 nmol of the TLR9 antagonist oligonucleotide ODN2088 or a negative control oligonucleotide was coinjected with 1×10^7 CFUs of *S. aureus*. Bacterial burden of each ear was $<1 \times 10^5$ CFUs per ear 6 h after only PBS was injected into ears of C57BL/6N mice and *Cxcl14*$^{-/-}$ mice. For stability and safety of cutaneous injection, we performed the operation at the same irradiance of about 150 lx both at daytime (ZT4) and nighttime (ZT16); operated mice were returned to the previous housing conditions after several minutes. For CFU determination, each infected ear was harvested after cervical dislocation 6 h postinjection. In some experiments, we collected infected ears 24 h after the injection. Ears were mechanically homogenized using a POLYTRON PT 2500 E (Kinematica) in PBS. Serial dilutions of ear homogenates were plated on LB agar plates. Plates were incubated at 37 °C overnight, and CFUs were counted the following day. To determine the effect of infection on chemokine induction at RNA levels in skin, we harvested mouse ears 3 h postinjection, and samples were kept in RNAlater Stabilization Solution (Thermo Fisher Scientific).

S. aureus DNA Binding Assay. Details of the plate-based binding assay used was described previously (37). *S. aureus* DNA (1 μg/mL) was applied to binding assay with or without ODN2395. Eluted DNA was purified with gel filtration for qPCR analysis using primer sets for the *S. aureus* Nuc gene region (*SI Appendix*, Table S1). For the binding assay for RAW264.7 cells, cells in 24-well plates were treated with *S. aureus* DNA in the presence or absence of 300 nM CXCL14 at 4 °C for 1 h. The treated cells were lysed to isolate genomic DNA. The copy ratio of *S. aureus* DNA to mouse genome DNA was determined by qPCR using primer sets for *S. aureus* Nuc [used for copy number validation (53)] and mouse rRNA (*SI Appendix*, Table S1).

LMD of the epidermis, immunohistochemistry, and in situ hybridization, EIA, regents, cell culture, HcCaT cell line expressing RORα, promoter–reporter assay, qRT-PCR, ELISA, FACS analysis, and phagocytic activity are available in method sections of *SI Appendix, Supplementary Text*.

Statistical Analysis. Statistical analyses were performed using Prism 8 software (GraphPad Software). Differences in *P* values between two treatment groups were determined using a two-tailed unpaired *t* test. The Kruskal–Wallis test or a two-way ANOVA with multiple comparisons (described in the corresponding figure legends) was used to determine statistical significance for comparison between three or more groups. $P < 0.05$ was considered statistically significant.

Peak time and amplitude values in qRT-PCR were obtained using a program written in R. To determine PS50 values, sigmoidal dose–response curves with *z* variable slope, $Y = \text{Bottom} + (\text{Top} - \text{Bottom})/(1 + 10(\log PS50 - X)\,\text{HillSlope})$, was fitted to the onset/offset time points (locomotor activity) or the peak time points (body temperature) using GraphPad Prism software. A statistically significant difference was assumed when *P* values were less than 0.05.

Author affiliations: [a]Graduate School of Pharmaceutical Sciences, Kyoto University, Kyoto 606-8501, Japan; [b]Department of Dermatology, Graduate School of Medicine, Kyoto University, Kyoto 606-8501, Japan; [c]Stem Cell Project, Tokyo Metropolitan Institute of Medical Science, Tokyo 156-8506, Japan; [d]Department of Pathology and Cell Regulation, Kyoto Prefectural University of Medicine, Kyoto 602-8566, Japan; [e]Graduate School of Frontier Biosciences, Osaka University, Osaka 565-0871, Japan; [f]Graduate School of Medical and Dental Sciences, Tokyo Medical and Dental University, Tokyo 113-8510, Japan; [g]Core Technology and Research Center, Tokyo Metropolitan Institute of Medical Science, Tokyo 156-8506, Japan; [h]Oral Health Science Research Center, Graduate School of Kanagawa Dental University, Kanagawa 238-8580, Japan; [i]Institute for the Advanced Study of Human Biology, Kyoto University Institute for Advanced Study, Kyoto University, Kyoto 606-8501, Japan; [j]The Hakubi Center for Advanced Research, Kyoto University, Kyoto 606-8501, Japan; [k]Department of Anatomy and Cell Biology, Graduate School of Medicine, Kyoto University, Kyoto 606-8501, Japan; [l]Department of Neuroscience, Graduate School of Medicine, Kyoto University, Kyoto 606-8501, Japan; and [m]Graduate School of Science, Department of Biological Science, Tokyo Metropolitan University, Tokyo 192-0397, Japan

1. V. Kumar, A. K. Abbas, J. C. Aster, *Robbins & Cotran Pothologic Basis of Disease* (Elsevier, Amsterdam, ed. 10, 2020).
2. F. O. Nestle, P. Di Meglio, J.-Z. Qin, B. J. Nickoloff, Skin immune sentinels in health and disease. *Nat. Rev. Immunol.* **9**, 679–691 (2009).
3. K. Kabashima, T. Honda, F. Ginhoux, G. Egawa, The immunological anatomy of the skin. *Nat. Rev. Immunol.* **19**, 19–30 (2019).
4. J. J. Bernard, R. L. Gallo, J. Krutmann, Photoimmunology: How ultraviolet radiation affects the immune system. *Nat. Rev. Immunol.* **19**, 688–701 (2019).
5. L. S. Miller, J. S. Cho, Immunity against *Staphylococcus aureus* cutaneous infections. *Nat. Rev. Immunol.* **11**, 505–518 (2011).
6. A. Abtin et al., Perivascular macrophages mediate neutrophil recruitment during bacterial skin infection. *Nat. Immunol.* **15**, 45–53 (2014).
7. E. D. Herzog, Neurons and networks in daily rhythms. *Nat. Rev. Neurosci.* **8**, 790–802 (2007).
8. E. E. Zhang, S. A. Kay, Clocks not winding down: Unravelling circadian networks. *Nat. Rev. Mol. Cell Biol.* **11**, 764–776 (2010).
9. J. S. Takahashi, Transcriptional architecture of the mammalian circadian clock. *Nat. Rev. Genet.* **18**, 164–179 (2017).
10. J. J. Loros, S. A. Denome, J. C. Dunlap, Molecular cloning of genes under control of the circadian clock in Neurospora. *Science* **243**, 385–388 (1989).
11. U. Schibler et al., Clock-talk: Interactions between central and peripheral circadian oscillators in mammals. *Cold Spring Harb. Symp. Quant. Biol.* **80**, 223–232 (2015).
12. R. Allada, J. Bass, Circadian mechanisms in medicine. *N. Engl. J. Med.* **384**, 550–561 (2021).
13. K. B. Koronowski, P. Sassone-Corsi, Communicating clocks shape circadian homeostasis. *Science* **371**, eabd0951 (2021).
14. J. Bass, Circadian topology of metabolism. *Nature* **491**, 348–356 (2012).
15. C. M. Greco, P. Sassone-Corsi, Circadian blueprint of metabolic pathways in the brain. *Nat. Rev. Neurosci.* **20**, 71–82 (2019).
16. T. Hara, K. Tanegashima, Pleiotropic functions of the CXC-type chemokine CXCL14 in mammals. *J. Biochem.* **151**, 469–476 (2012).
17. M. Hernández-Ruiz, A. Zlotnik, Mucosal chemokines. *J. Interferon Cytokine Res.* **37**, 62–70 (2017).
18. A. Zlotnik, A. M. Burkhardt, B. Homey, Homeostatic chemokine receptors and organ-specific metastasis. *Nat. Rev. Immunol.* **11**, 597–606 (2011).
19. W. J. Schwartz, S. M. Reppert, Neural regulation of the circadian vasopressin rhythm in cerebrospinal fluid: A pre-eminent role for the suprachiasmatic nuclei. *J. Neurosci.* **5**, 2771–2778 (1985).
20. X. Jin et al., A molecular mechanism regulating rhythmic output from the suprachiasmatic circadian clock. *Cell* **96**, 57–68 (1999).
21. J. D. Li, K. J. Burton, C. Zhang, S. B. Hu, Q. Y. Zhou, Vasopressin receptor V1a regulates circadian rhythms of locomotor activity and expression of clock-controlled genes in the suprachiasmatic nuclei. *Am. J. Physiol. Regul. Integr. Comp. Physiol.* **296**, R824–R830 (2009).
22. Y. Yamaguchi et al., Mice genetically deficient in vasopressin V1a and V1b receptors are resistant to jet lag. *Science* **342**, 85–90 (2013).
23. Y. Nakahata, S. Sahar, G. Astarita, M. Kaluzova, P. Sassone-Corsi, Circadian control of the NAD+ salvage pathway by CLOCK-SIRT1. *Science* **324**, 654–657 (2009).
24. K. M. Ramsey et al., Circadian clock feedback cycle through NAMPT-mediated NAD+ biosynthesis. *Science* **324**, 651–654 (2009).
25. M. Tanioka et al., Molecular clocks in mouse skin. *J. Invest. Dermatol.* **129**, 1225–1231 (2009).
26. K. Tanegashima et al., CXCL14 acts as a specific carrier of CpG DNA into dendritic cells and activates Toll-like receptor 9-mediated adaptive immunity. *EBioMedicine* **24**, 247–256 (2017).
27. S. Méndez-Ferrer, D. Lucas, M. Battista, P. S. Frenette, Haematopoietic stem cell release is regulated by circadian oscillations. *Nature* **452**, 442–447 (2008).
28. P. Hevezi et al., Genome-wide analysis of gene expression in primate taste buds reveals links to diverse processes. *PLoS One* **4**, e6395 (2009).
29. C. Maerki et al., Potent and broad-spectrum antimicrobial activity of CXCL14 suggests an immediate role in skin infections. *J. Immunol.* **182**, 507–514 (2009).
30. P. Schaerli, K. Willimann, L. M. Ebert, A. Walz, B. Moser, Cutaneous CXCL14 targets blood precursors to epidermal niches for Langerhans cell differentiation. *Immunity* **23**, 331–342 (2005).
31. S. Y. C. Tong, J. S. Davis, E. Eichenberger, T. L. Holland, V. G. Fowler Jr., *Staphylococcus aureus* infections: Epidemiology, pathophysiology, clinical manifestations, and management. *Clin. Microbiol. Rev.* **28**, 603–661 (2015).
32. A. P. Kourtis et al.; Emerging Infections Program MRSA author group, Vital signs: Epidemiology and recent trends in methicillin-resistant and in methicillin-susceptible *Staphylococcus aureus* bloodstream infections–United States. *MMWR Morb. Mortal. Wkly. Rep.* **68**, 214–219 (2019).
33. H. W. Boucher, G. R. Corey, Epidemiology of methicillin-resistant *Staphylococcus aureus*. *Clin. Infect. Dis.* **46** (suppl. 5), S344–S349 (2008).
34. C. Scheiermann, Y. Kunisaki, P. S. Frenette, Circadian control of the immune system. *Nat. Rev. Immunol.* **13**, 190–198 (2013).
35. A. M. Curtis, M. M. Bellet, P. Sassone-Corsi, L. A. O'Neill, Circadian clock proteins and immunity. *Immunity* **40**, 178–186 (2014).
36. K. Man, A. Loudon, A. Chawla, Immunity around the clock. *Science* **354**, 999–1003 (2016).
37. R. Iwase et al., Identification of functional domains of CXCL14 involved in high-affinity binding and intracellular transport of CpG DNA. *J. Immunol.* **207**, 459–469 (2021).

38. A. C. Silver, A. Arjona, W. E. Walker, E. Fikrig, The circadian clock controls toll-like receptor 9-mediated innate and adaptive immunity. *Immunity* **36**, 251–261 (2012).

39. T. Hasegawa *et al.*, Reduction in human epidermal Langerhans cells with age is associated with decline in CXCL14-mediated recruitment of CD14(+) monocytes. *J. Invest. Dermatol.* **140**, 1327–1334 (2020).

40. Marmoset Genome Sequencing and Analysis Consortium, The common marmoset genomeprovides insight into primate biology and evolution. *Nat. Genet.* **46**, 850–857 (2014).

41. H. G. Erkert, Characteristics of the circadian activity rhythm in common marmosets (*Callithrix j. jacchus*). *Am. J. Primatol.* **17**, 271–286 (1989).

42. T. D. Shellenberger *et al.*, BRAK/CXCL14 is a potent inhibitor of angiogenesis and a chemotactic factor for immature dendritic cells. *Cancer Res.* **64**, 8262–8270 (2004).

43. J. Gibbs *et al.*, An epithelial circadian clock controls pulmonary inflammation and glucocorticoid action. *Nat. Med.* **20**, 919–926 (2014).

44. C. Dai *et al.*, CXCL14 displays antimicrobial activity against respiratory tract bacteria and contributes to clearance of *Streptococcus pneumoniae* pulmonary infection. *J. Immunol.* **194**, 5980–5989 (2015).

45. K. Tanegashima *et al.*, CXCL14 deficiency in mice attenuates obesity and inhibits feeding behavior in a novel environment. *PLoS One* **5**, e10321 (2010).

46. H. Hemmi *et al.*, A Toll-like receptor recognizes bacterial DNA. *Nature* **408**, 740–745 (2000).

47. R. Hata *et al.*, Suppressed rate of carcinogenesis and decreases in tumour volume and lung metastasis in CXCL14/BRAK transgenic mice. *Sci. Rep.* **5**, 9083 (2015).

48. G. T. J. van der Horst *et al.*, Mammalian Cry1 and Cry2 are essential for maintenance of circadian rhythms. *Nature* **398**, 627–630 (1999).

49. T. Matsuo *et al.*, Control mechanism of the circadian clock for timing of cell division in vivo. *Science* **302**, 255–259 (2003).

50. A. Maeda *et al.*, Circadian intraocular pressure rhythm is generated by clock genes. *Invest. Ophthalmol. Vis. Sci.* **47**, 4050–4052 (2006).

51. K. Tanegashima *et al.*, Epigenetic regulation of the glucose transporter gene Slc2a1 by β-hydroxybutyrate underlies preferential glucose supply to the brain of fasted mice. *Genes Cells* **22**, 71–83 (2017).

52. H. Liu *et al.*, *Staphylococcus aureus* epicutaneous exposure drives skin inflammation via IL-36-mediated T cell responses. *Cell Host Microbe* **22**, 653–666.e5 (2017).

53. A. Haque *et al.*, Rapid screening of pyogenic *Staphylococcus aureus* for confirmation of genus and species, methicillin resistance and virulence factors by using two novel multiplex PCR. *Pak. J. Med. Sci.* **33**, 1095–1100 (2017).